CrossMark

ORIGINAL PAPER

Preparation of nanocellulose/filter paper (NC/FP) composite membranes for high-performance filtration

Zhiguo Wang · Wenwen Zhang · Juan Yu · Lijun Zhang · Liang Liu · Xiaofan Zhou · Chaobo Huang · Yimin Fan

Abstract A layer deposition method was developed to prepare a series of nanocellulose/filter paper (NC/FP) composite filtration membranes by vacuum filtration of an aqueous nanocellulose dispersion on a filter paper substrate. The deposited NC networks and the final pore structure of the NC/FP composite were affected by the size and the amount of the nanocellulose. Drying methods further influenced the filtration performance of the membranes. With a greater NC aspect ratio and an increasing amount of added NC, NC/FP composite membranes exhibited better rejection rates with lower water flux. Two types of NC were chosen with different sizes as follows: (1) cellulose nanocrystals prepared from microcrystalline cellulose, which are characterized by their small size, and (2) cellulose nanofibers (CNFs) prepared from hardwood bleached Kraft pulp, which are characterized by their large size. Varying filtration performance was also achieved by altering the drying conditions (temperature, pressure and solvents) during the manufacturing process of NC/FP composite filtration membranes. In particular, NC/FP composite membranes obtained by vacuum drying at 60 °C with 0.1% CNFs demonstrated excellent ultrafiltration properties with retention rates as high as 97.14% and an acceptable flux ($46,279 \ \mathrm{L \ m^{-2} \ h^{-1}}$). Furthermore, NC/FP composite membranes demonstrated good tolerance to acidic and alkaline conditions, but their performance was weakened when treated with high or low temperatures. NC/FP composite membranes have promising potential for use as advanced separation membranes for water purification.

Z. Wang · W. Zhang · J. Yu · L. Zhang ·
L. Liu · X. Zhou · C. Huang · Y. Fan
Jiangsu Co-Innovation Center of Efficient Processing and Utilization of Forest Resources, College of Light Industry and Food Engineering, College of Chemical Engineering, Nanjing Forestry University, Nanjing 210037, China

Y. Fan (✉)
Jiangsu Key Lab of Biomass-Based Green Fuel and Chemicals, College of Chemical Engineering, Nanjing Forestry University, Nanjing 210037, China
e-mail: fanyimin@njfu.edu.cn

Graphical abstract
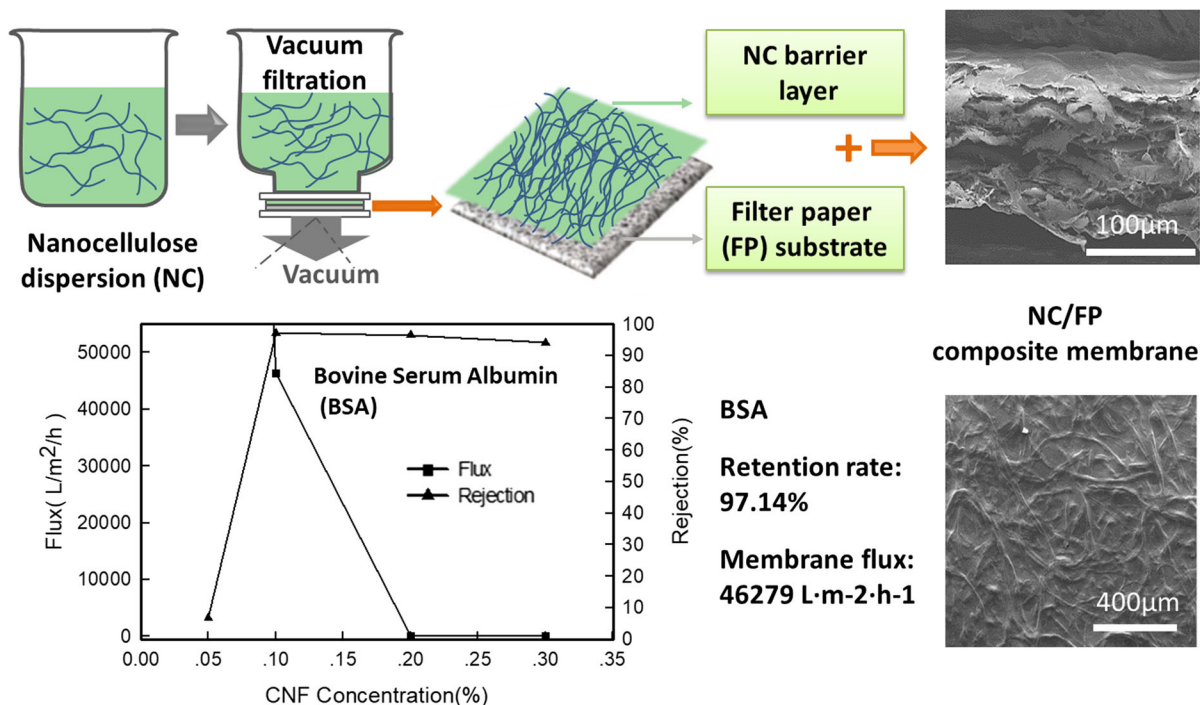
Introduction

With the deterioration of the ecological environment, materials separation has become one of the most important areas of research, and membrane separation technology is also considered one of the most important technologies (Van Reis and Zydney 2001). Ultrafiltration (UF) membranes are particularly important in membrane separation research and are widely used in wastewater treatment and the medical and food industries (Jelen 1998). However, large quantities of solvents, chemicals and energy (Henmi et al. 2012; Mungray and Murthy 2012) are required to produce UF membranes. Therefore, it is important to develop new membrane materials and investigate simplified processes to produce UF membranes.

Composite membranes are usually used for ultrafiltration membranes. In a composite structure, the thickness of a film layer that is used for separation is greatly reduced, thereby reducing the mass transfer resistance and increasing the flux of the membrane. In addition, the mechanical and anti-swelling properties of the membrane are enhanced (Pesek and Koros 1994; Wessling et al. 2001; Cadotte et al. 1980). Vacuum extraction is the most direct and convenient method for preparing composite membranes. Karan et al. (2012) prepared ultrathin diamond-like nano-films on a support layer with large pores through a direct filtration method. The aperture of the ultrathin film was l nm, the film flux was very high, and it exhibited good mechanical properties. According to the Carman–Kozeny filtration theory, the flux of an ultrafiltration membrane is inversely proportional to the thickness of its effective separation layer. In other words, thinner separation layers provide a larger membrane flux (Bowen and Jenner 1995). Therefore, ultrathin ultrafiltration membranes are the most effective way to prepare high-flux separation membranes. Compared to traditional commercial ultrafiltration membranes, ultrathin composite membranes prepared by direct filtration have advantages, including ultra-high flux and small film resistance, and can be widely used in industrial applications.

Cellulose fibers are excellent raw materials for the production of UF membranes (Baker 1981; Ma et al. 2010) because of their outstanding mechanical and chemical properties (Klemm et al. 2011; Chen et al. 2010; Ling et al. 2018a, b; Yang et al. 2018) and their capacity to develop many materials with different structures and properties (Moon et al. 2011; Ling et al. 2018a, b). Saito et al. successfully prepared cellulose nanofibers with a diameter of 3–4 nm and a micron-scale length from natural plant cellulose by a TEMPO-mediated oxidation method (Saito et al. 2006; Isogai et al. 2018). The cellulose nanofibers had a high aspect ratio and mechanical strength and a low thermal expansion rate (0.1 PPM/K) and density (1.6 g cm^{-3}) (Jakob et al. 1995; Nishino et al. 1995; Yano et al. 2010) and could be used as a raw material to prepare nanopaper and films (Siró and Plackett 2010). Nanopaper possesses pores in the nanometer range and could potentially be used in separation applications (Mautner et al. 2014; Chun et al. 2012). Cellulose nanofibers (CNFs) are also widely used in the fabrication of nanocomposite membranes for water treatment technologies (Carpenter et al. 2015; Ma et al. 2014; Thakur and Voicu 2016; Ma et al. 2011a, b). Many membranes have been produced by incorporating CNF with a variety of polymer matrices, including chitosan (Karim et al. 2014), cellulose triacetate (Kong et al. 2014; Soeta et al. 2015), poly(vinylidene fluoride) (PVDF) (Lv et al. 2018), poly(vinyl alcohol) (PVA) (Wang et al. 2013; Xu et al. 2013), poly(acrylonitrile) (PAN) (Ma et al. 2011a, b), polypyrrole (PPy) (Ferraz et al. 2013), poly(HEMA) and poly(AAS) (Wang et al. 2017). The tensile strength, surface hydrophilicity, permeability and resistance to biofouling of a membrane has been improved by adding a small weight percentage of CNFs. Sun et al. (2015) also used oxidized cellulose nanocrystals (CNCs) as a strengthening additive for paper and in applications as a sustainable, wet-strength additive.

Moreover, some research has shown that solvent treatment [such as ethanol treatment (Liu et al. 2018) and acetone treatment (Karim et al. 2016)] of the membranes prior to drying reduced interchain H-bonding, resulting in an increase in the rejection rate and water flux of the fabricated membranes. Additionally, different types of nanocellulose were used to produce nanopaper-based membranes and were able to control the pore sizes of the resultant nanopaper (Mautner et al. 2015). Furthermore, nanocellulose with different diameters and lengths may be used to produce different membranes for a wide range of potential applications.

In this work, we used a layer deposition method facilitated by vacuum filtration to prepare ultrafiltration membranes with filter paper (FP) as a support membrane and nanocellulose (NC) as a surface-barrier layer. This proposed method can be used to prepare inexpensive NC/FP composite filtration membranes with a simple production process to give materials with excellent performance abilities. There is great potential for the application of these methods and materials in the preparation of ultrafiltration (UF) membranes.

Materials and methods

Materials

Commercial HBKP (bleached acacia Kraft pulp produced by Asia Symbol Pulp and Paper Co., Ltd., Shandong, China) with an α-cellulose content of ∼ 80% was used as the wood cellulose sample. Microcrystalline cellulose (MCC) was purchased from Sinopharm Chemical Reagent Co., Ltd. The 2,2,6,6-tetramethylpiperidine-1-oxyl radical (TEMPO, 98%) was purchased from Sigma. Sodium hypochlorite solution (7–10% in chlorine) was purchased from Sigma-Aldrich. Sodium bromide was obtained from Fisher Scientific. All other reagents were of analytical grade and used without further purification from Nanjing Chemical Reagent Co., Ltd.

Preparation of TEMPO-oxidized cellulose nanofibers (CNFs) and nanocrystals (CNCs)

To prepare cellulose nanofibers (CNFs) and cellulose nanocrystals (CNCs) with different aspect ratios, HBKP and MCC were used as the raw materials, respectively. HBKP or MCC (1 g) was suspended in a beaker in which designated amounts of TEMPO (0.016 g) and sodium bromide (0.1 g) were dissolved. Then, the desired amount of a sodium hypochlorite (NaClO) solution (6 mmol) was added to the mixture. The pH of the mixture was maintained at 10 by the continuous addition of 0.5 M NaOH using a pH-Stat titration system. The reaction was quenched by adding

ethanol and then 0.5 M hydrochloric acid (HCl) dropwise to adjust the pH to 7, and the reaction stopped when no consumption of the base was observed.

After oxidation, the mixture was washed with distilled water by repeated centrifugation (more than 6 times) at 8228 g for 6 min to obtain TEMPO-oxidized cellulose as a water-insoluble fraction. A 0.1% (w/v) suspension of TEMPO-oxidized cellulose was sonicated using an ultrasonic homogenizer (VCX500, Sonics and Materials, Inc., USA) at 500 W and 20 kHz for 20 min with start/stop intervals to avoid increasing the temperature. The diameter of the homogenizer tip was 1.2 cm. After centrifugation at 12,857 g for 6 min to remove the nonfibrillated fraction, TEMPO-oxidized CNFs or CNCs were obtained as the supernatant dispersed in water.

Preparation of nanocellulose/filter paper (NC/FP) composite membranes

A schematic of the fabrication procedure of NC/FP composite membranes is shown in Fig. 1. The NC/FP composite membranes were prepared through the filtration of an aqueous nanocellulose dispersion with filter paper as the substrate. Using a solvent filter with medium-speed quantitative filter paper as the substrate, below which was a layer of a 0.1 μm nylon filter membrane, the nanocellulose dispersion at different concentrations was deposited on the filter membrane through direct filtration.

Analysis and characterization of nanocellulose

Fourier transform infrared (FT-IR) spectra of the nanocellulose were obtained with an infrared spectrometer (VERTEX 80 V, Bruker, Germany) from 4000 to 400 cm^{-1}. The samples were freeze-dried before measurements were conducted.

The X-ray diffraction (XRD) patterns of nanocellulose were obtained at ambient temperature by step-scanning on an X-ray powder diffractometer (Ultima IV, Japan) using monochromatic Cu Kα radiation ($\lambda = 1.54$ Å) in the range of $2\theta = 5°–50°$ with a step size of $0.02°$ and a scanning rate of $5°$ min^{-1}. The samples were freeze-dried before measurements were conducted.

Atomic force microscopy (AFM) images were obtained using a Dimension Edge microscope (Bruker) in light tapping mode. V-shaped silicon cantilevers (Micromash) with a nominal tip radius of 8 nm were used for imaging. The samples were air-dried in a diluted dispersion (below 1/10,000 dilution) and then dropped onto mica before measurements were conducted.

Analysis and characterization of NC/FP composite membranes

Thermogravimetric analysis (TGA) (with a model HTC-3 instrument from Beijing Permanent Scientific Instrument Factory) scans of samples were collected at 10 °C min^{-1} from 25 to 700 °C min^{-1} under a 50 mL min^{-1} air flow. The samples were freeze-dried before measurements were conducted.

The thermal resistance of the NC/FP composite membranes was tested by placing NC/FP composite membranes in an 80 °C water bath and a − 20 °C freezer for 3 h each and then measuring their pure water flux.

The acid and alkaline resistances of NC/FP composite membranes were evaluated by immersing NC/FP composite membranes a 0.5 mol L^{-1} hydrochloric acid or 0.5 mol L^{-1} sodium hydroxide solution for 24 h and then washing them with distilled water. The

Fig. 1 Schematic of the fabrication procedure of NC/FP composite membranes
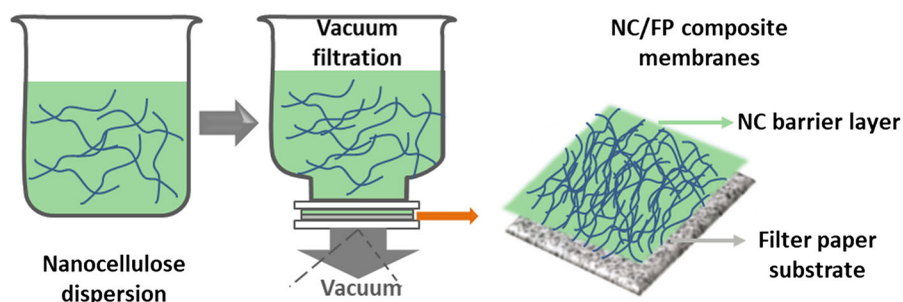
pure water flux was measured before and after treatment to test the acid and alkaline resistances of the filters.

The morphologies of the NC/FP composite membranes were observed with a field emission scanning electron microscope (JSM-7600FESEM, Japan) and an environmental scanning electron microscope (ESEM) (Quanta 200, FEI) at an accelerating voltage of 15 kV. Prior to SEM imaging, samples were sputter-coated with gold for 90 s.

The performance of as-prepared composite membranes was evaluated by measuring the flux, rejection rate and porosity of NC/FP composite membranes.

NC/FP composite membrane flux was tested at room temperature with a pressure of 0.1 MPa. The results were calculated according to the following equation:

$$Jw = V/(T*A), \tag{1}$$

where V is the volume of the filtered fluid, T is the sampling time and A is the effective area of the membrane.

The rejection performance of NC/FP composite membranes was tested using a 1 g L^{-1} aqueous solution of bovine serum albumin (BSA). The absorbance of the liquid and filtrate were measured with a UV–Vis spectrometer (UV-1800 2100Qis, HACH). The rejection rate was calculated by the following equation:

$$R = (1-C_1/C_2)*100\%, \tag{2}$$

where C_2 and C_1 represent the concentration of the liquid before and after filtration, respectively.

The porosity was calculated as the ratio of the pore volume to the total volume in the membrane. The porosity of the membranes was calculated with the following formula:

$$Pr = (m_2-m_1)/V/\rho, \tag{3}$$

where m_1 and m_2 are the weight of the membranes before and after absorbing ethanol, respectively, V is the volume of the membrane and ρ is the density of ethanol.

Results and discussion

Analysis and characterization of nanocellulose (CNFs and CNCs)

The TEMPO-oxidized hardwood bleached Kraft pulp (HBKP) and microcrystalline cellulose (MCC) were detected in the FT-IR spectra, as shown in Fig. 2a. After oxidation, additional absorption bands at approximately 1730 cm^{-1} appeared, corresponding to the C=O stretching vibration of carboxyl groups (Habibi et al. 2006), which indicated that carboxyl groups were introduced into the HBKP and MCC after TEMPO oxidation.

The X-ray diffraction patterns of HBKP and MCC before and after TEMPO-oxidation were determined to investigate their crystal structures, as shown in Fig. 2b. The peaks at $2\theta = 14°–18°$, $22.5°$, and $34.5°$ are characteristic of cellulose I (Klemm et al. 2005). A comparison of this data with the crystal structure of cellulose I in the samples before oxidation indicates that there were no apparent changes in the TEMPO-oxidized samples, which indicates that the carboxylate groups formed during oxidation were present only on the surface of the nanocrystals, without any internal cellulose crystals (Isogai et al. 2018).

CNFs and CNCs prepared from TEMPO-oxidized HBKP and MCC, respectively, were observed using atomic force microscopy, and their morphologies are shown in Fig. 2c, d. After oxidation and sonication, the fiber sizes were uniform and evenly distributed. The average diameters of the CNFs were approximately 4–20 nm, and their lengths ranged up to the micrometer scale. Because of their high length to diameter ratio, these materials make a perfect filter composite. The average diameters and lengths of the CNCs were approximately 3–15 nm and 100–400 nm, respectively. The fibers were shorter and were tubular in shape.

The effects of nanocellulose concentration and size (CNFs or CNCs) on the water flux of NC/FP composite membranes

The pure water fluxes of NC/FP composite membranes obtained by air drying at different NC concentrations were investigated (Fig. 3). The fluxes of all NC/FP composite membranes were smaller than those of the filter paper (294,120 L m^{-2} h^{-1}). With increasing NC

Fig. 2 FT-IR (**a**) and XRD (**b**) spectra of TEMPO-oxidized HBKP and MCC, AFM images of CNFs prepared from TEMPO-oxidized HBKP (**c**) and CNCs prepared from TEMPO-oxidized MCC (**d**)
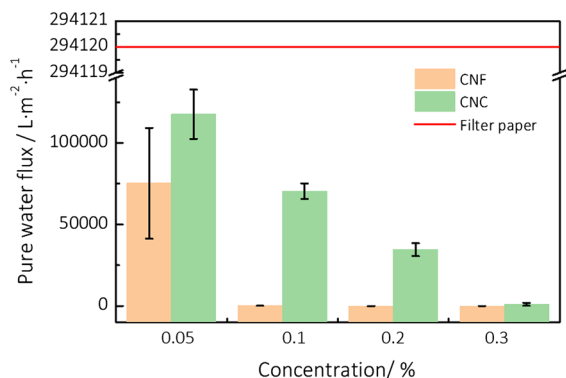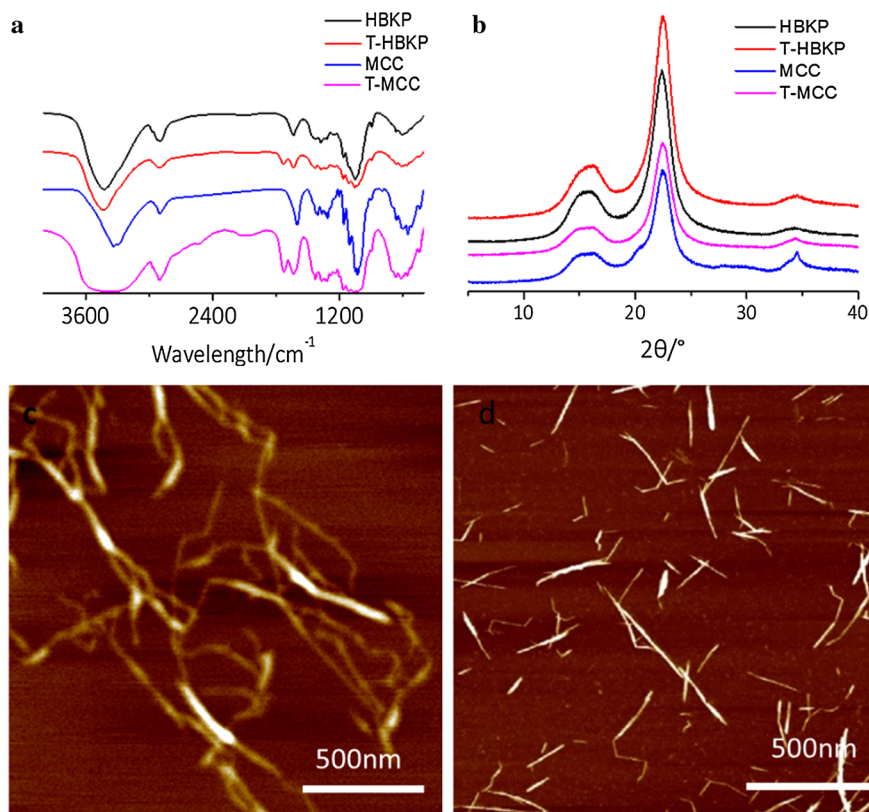

Fig. 3 Effects of the concentration of nanocellulose (CNFs or CNCs) on the water flux of NC/FP composite membranes

concentration, the water flux decreased gradually. The SEM images of NC/FP composite membranes with different NC concentrations demonstrate this phenomenon (Fig. 4 and Fig. S1). The raw filter paper fibers were intertwined to form a porous network, in which thick fibers formed scaffolds and fine fibers provided surface area. The substrate was deposited and covered with a layer of NC (CNFs or CNCs)

during the preparation of composite membranes. With an increased NC concentration, the NC surface layer gradually covered the coarse fibers, and the surface layer became thicker and denser, which led to a decrease in the water flux. In addition, the fluxes of the composite membrane prepared using CNCs were much greater than CNFs prepared under the same conditions. Because of the shorter nanocrystals and lower aspect ratios of CNCs, the fibers did not effectively overlap, which resulted in CNC/FP composite membranes with larger pores (Fig. 4), such that the membranes were able to filter water quickly. We found that the CNC/FP composite with these characteristics is more favorable as a microfiltration membrane (data not shown here). Therefore, the properties of CNF/FP composite membranes, which are speculated to be more favorable for the formation of ultrafiltration membranes, were further investigated and discussed in this study.
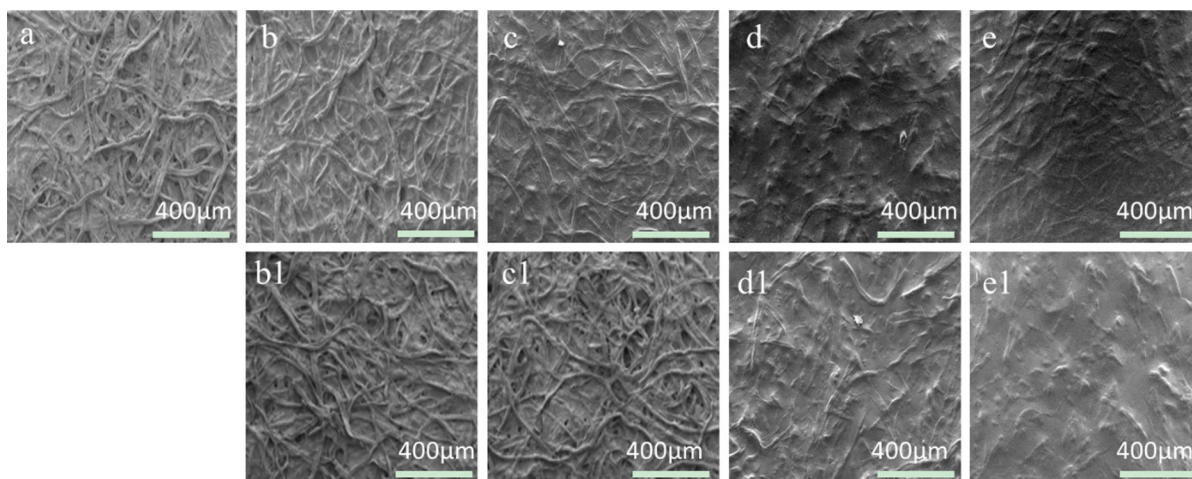
Fig. 4 SEM images of CNF/FP (**a**–**e**) and CNC/FP (**b**1–**e**1) composite membrane surfaces with different NC concentrations [0% (**a**), 0.05% (**b**, **b**1), 0.1% (**c**, **c**1), 0.2% (**d**, **d**1), 0.3% (**e**, **e**1)]

The effect of drying conditions on the water flux of CNF/FP composite membranes

The air-drying process resulted in very strong hydrogen bonding between water molecules and cellulose molecules. As free water evaporates, the tension that is produced is large enough to shorten the distance between cellulose molecules and form new intermolecular hydrogen bonds between the fibers. Therefore, the pore structures of the wet membranes after natural drying will collapse, causing problematic densification of the membrane structure. However, CNF/FP composite membranes produced under negative pressure might maintain their original pore structures. Therefore, CNF/FP composite membranes were obtained by vacuum drying. As the temperature during vacuum drying increased to 60 °C, the high temperature resulted in the rapid evaporation of water, which caused the membrane structure to be fixed before the formation of aggregate structures through intermolecular interactions. As a result, the membranes obtained by vacuum drying at 60 °C had a significantly greater water flux (Fig. 5a, b) than those obtained under the other drying conditions. CNF/FP composite membranes obtained by freeze-drying had many noticeable defects, such as bubbles or wrinkles on the surface (Fig. S2). The water content of CNFs and FP is different; therefore, a gap between CNFs and FP was formed in CNF/FP composite membranes during the freezing process. This is attributed to the formation of bubbles or wrinkles during the

subsequent vacuum-drying process. Therefore, the performance of CNF/FP composite membranes was improved by vacuum drying at 60 °C.

In addition to drying methods and conditions, solvent displacement methods also affect the membrane performance because there are certain interactions between cellulose macromolecules and different solvents that yield different structures of the resultant CNF/FP composite membranes. The results proved that different solvent displacement methods produce CNF/FP composite membranes with fluffy textures in not only the CNF layer but also the filter paper substrate, therefore, making the pure water flux even greater than that of the original filter paper (Fig. 5c, d).

The surface and cross-sectional SEM images of CNF/FP composite membranes obtained by different drying methods demonstrated coinciding results (Fig. 6 and Fig. S3). The surfaces of CNF/FP composite membranes were relatively smooth and dense. The structure of CNF/FP composite membranes obtained by vacuum drying at 60 °C was less dense than the structure obtained by air drying, and the filter paper had a less compact CNF layer, which caused a higher water flux. After solvent displacement, the surface of the nanofiber thin film layer contained traces of the base membrane fibers, which shows that the layers are very close and will not be separated under normal circumstances. The cross-sectional images of the membranes show that the pores of the filter paper substrate became fluffier, such that its flux increased compared with that of the original

Fig. 5 Effects of drying conditions on the water flux of CNF/FP composite membranes
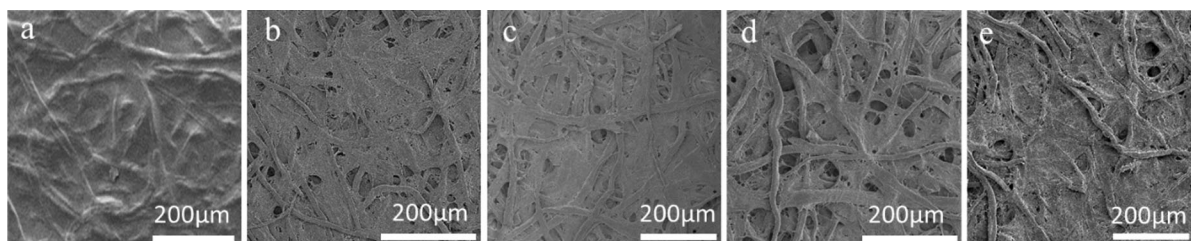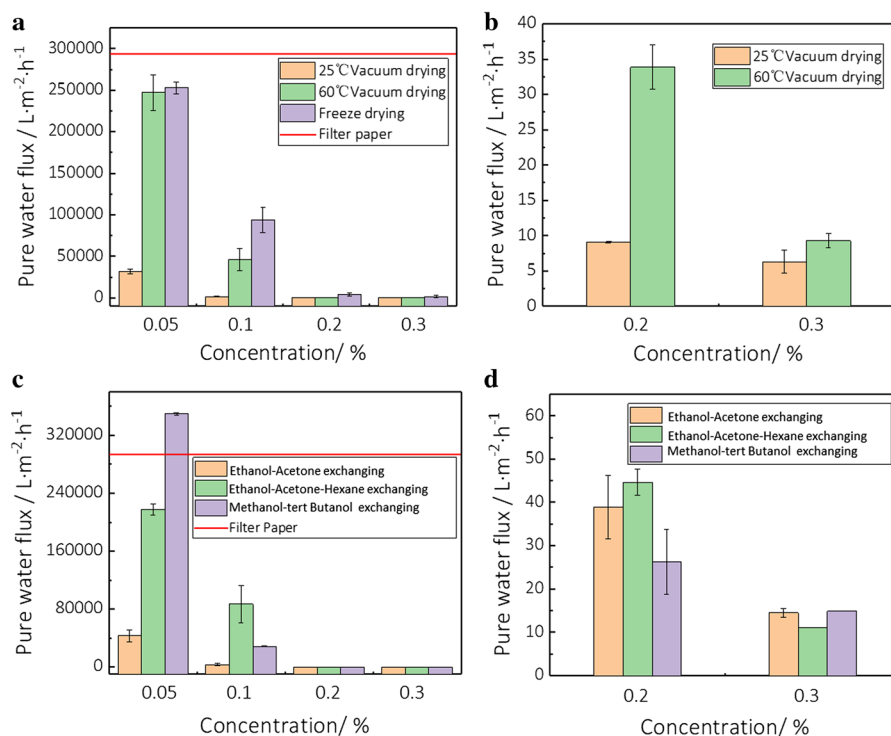

Fig. 6 SEM images of the surfaces of CNF/FP composite membranes (0.1% CNFs) obtained by different drying methods (**a** air drying, **b** vacuum drying at 60 °C, **c** ethanol-acetone exchange, **d** ethanol-acetone-hexane exchange and **e** methanol-*tert*-butanol exchange)

filter paper, which is also related to the retention performance of CNF/FP composite membranes.

The porous structure of the membrane is one of the kinetic parameters that defines its permeability. The porosities of different CNF/FP composite membranes are shown in Table 1. As the CNF concentration increased, the porosity of the CNF/FP composite membranes gradually decreased, which is in agreement with the change in flux of CNF/FP composite membranes. The porosity of the filter paper that was used as the substrate matrix was 50.40%. The porosities of CNF/FP composite membranes obtained by different drying methods were all lower than that of the pure filter paper, especially for air drying and

vacuum drying at 25 °C, due to the increase in the density of the membrane. However, the porosities of CNF/FP composite membranes obtained by air drying after different solvent exchange processes were greater than those of the filter paper when the concentration of CNFs was low. This phenomenon indicates that solvent exchange not only keeps the pore structures of CNF/FP composite membranes but also makes the pore structures of the supporting layer expand slightly. Therefore, the pure water flux after the displacement of solvent and drying is greater.

Table 1 The porosity of different CNF/FP composite membranes

Drying method	Porosity at different CNF concentrations (%)			
	0.05	0.1	0.2	0.3
Air drying	46.89 ± 1.21	43.57 ± 2.21	43.65 ± 0.95	38.35 ± 1.30
25 °C vacuum drying	45.68 ± 0.85	42.36 ± 1.28	42.72 ± 1.36	36.23 ± 1.63
60 °C vacuum drying	48.30 ± 1.15	43.65 ± 0.96	34.48 ± 2.05	36.33 ± 0.75
Ethanol-acetone exchange	53.05 ± 2.01	55.19 ± 2.55	50.41 ± 1.87	50.06 ± 1.66
Ethanol-acetone-hexane exchange	57.18 ± 0.93	58.19 ± 1.48	50.62 ± 1.21	45.91 ± 0.82
Methanol-*tert*-butanol exchange	56.45 ± 1.54	55.64 ± 1.77	53.92 ± 1.27	47.97 ± 1.25

The effect of drying conditions on the rejection performance of CNF/FP composite membranes

The effect of CNF concentration on the flux and rejection performance of BSA on CNF/FP composite membranes obtained by different drying methods is shown in Fig. 7. A small amount of nanofiber changed the pure water flux of the CNF/FP composite membranes and captured impermeable species. As the amount of CNF increased, the flux decreased, and the rejection increased. When the concentration of CNFs was 0.1%, CNF/FP composite membranes not only had a high membrane flux but also showed good retention of BSA. Especially in the case of vacuum drying at 60 °C, when the CNF concentration was 0.1%, the rejection rate was as high as 97.14%, the membrane flux was maintained at a high level of 46,279 L m^{-2} h^{-1} and the overall performance of the membrane was extremely good (up to the level of ultrafiltration membranes).

When CNF/FP composite membranes were treated by solvent exchange, because of its loosened structure, the water flux after solvent exchange was higher than that of the membranes obtained by air drying (Fig. 6 and Fig. S4). After ethanol/acetone exchange, when the CNF concentration was 0.1%, the capture rate for BSA was 64.46%. When CNF/FP composite membranes were subjected to solvent exchange by either ethanol/acetone/hexane or methanol/*tert*-butanol, the concentrations of CNFs required for good retention and high membrane flux were between 0.1 and 0.2%. Considering the various drying methods that were investigated, CNF/FP composite membranes obtained by vacuum drying at 60 °C had favorable performance as ultrafiltration membranes.

Stability of CNF/FP composite membranes

By thermogravimetric analysis, we found that the TG curves of CNF/FP composites membrane (Fig. 8) were between the curves of filter paper and CNFs. However, because of the small proportion of CNFs, the TG curve was closer to the filter paper curve. The thermal stability of CNFs is worse than that of filter paper, which is stable at 320 °C. When the filter paper began to lose weight, 55% of CNFs were lost. In the TEMPO-oxidation process, beta-elimination was observed under alkaline conditions. Factors such as smaller size, increase in specific surface area and introduction of carboxyl groups to the surface of the cellulose molecules caused endothermic decomposition at lower temperatures.

The results of temperature, acidity and alkalinity tolerance tests of CNF/FP composite membranes are shown in Table 2. The pure water flux of CNF/FP composite membranes increased either positively or negatively compared with untreated CNF/FP composite membranes. The high temperature treatment caused an increase in the nanofiber cortices, and fiber–fiber junctions shifted to increase the pore diameters of the cortex; however, the low temperature treatment caused partial separation between the CNF/FP composite membrane cortex and the supporting layer. The acidic and alkaline treatments influenced the pores of the paper substrate, but the filtering effect and filtration velocity were determined by the surface of the CNF filtration layer. Therefore, the influences of acidic and alkaline treatments were less prominent than that of the temperature.
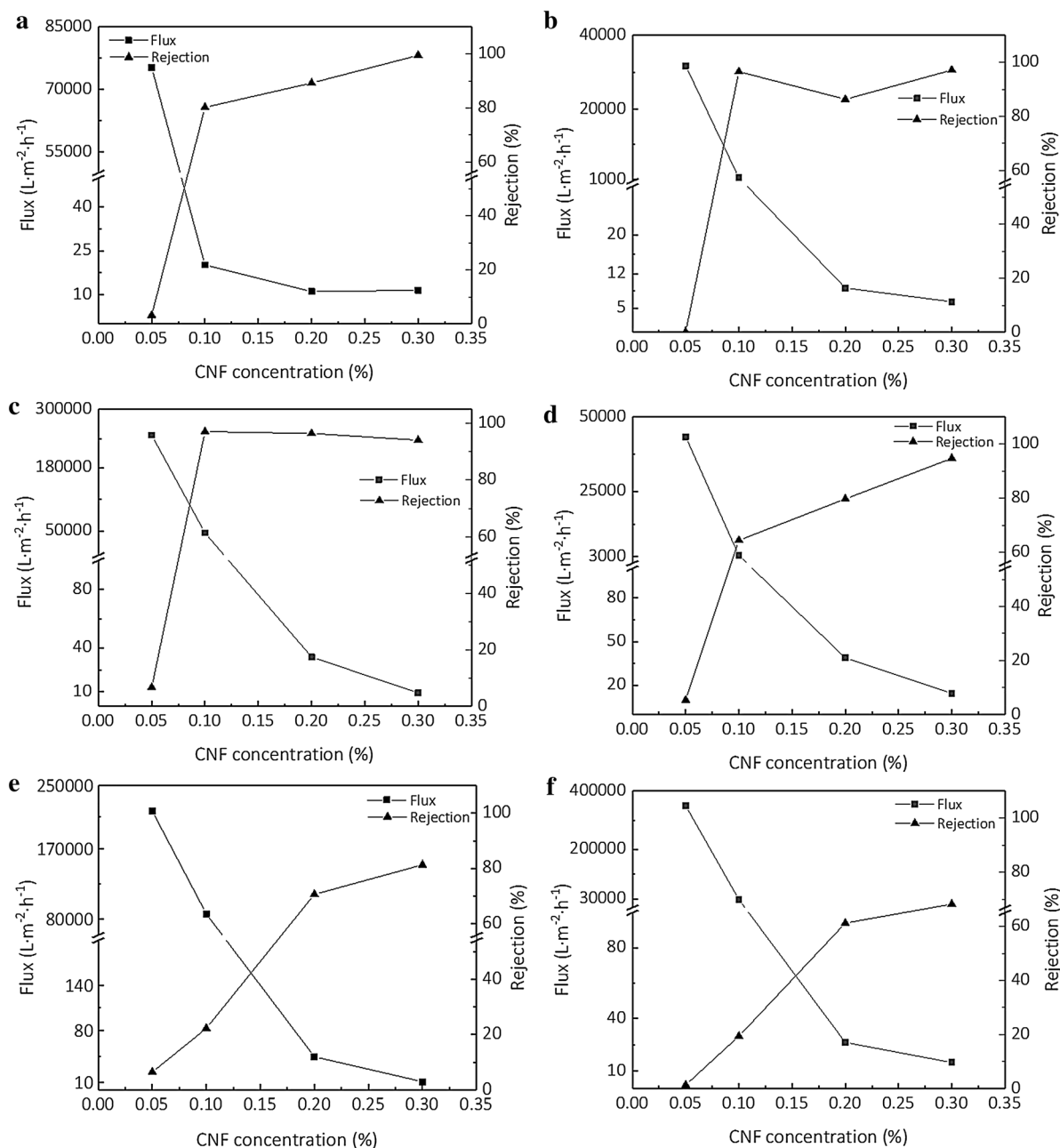
Fig. 7 Effect of CNF concentration and drying methods on the flux and rejection performance of BSA on CNF/FP composite membranes (**a** air drying, **b** vacuum drying at 25 °C, **c** vacuum drying at 60 °C, **d** ethanol-acetone exchange, **e** ethanol-acetone-hexane exchange and **f** methanol-*tert*-butanol exchange)

Conclusions

Nanocellulose (NC) layer deposited filter paper composite membranes using CNFs (prepared from HBKP) or CNCs (prepared from MCC) and filter paper (FP) were manufactured by a vacuum drying method.

Because of their varying sizes, different sources of nanocellulose influenced the comprehensive performance of NC/FP composite membranes. The aspect (length to diameter) ratio of CNFs was very high, and its filaments were intertwined on the filter paper substrate, which formed a mesh structure that was
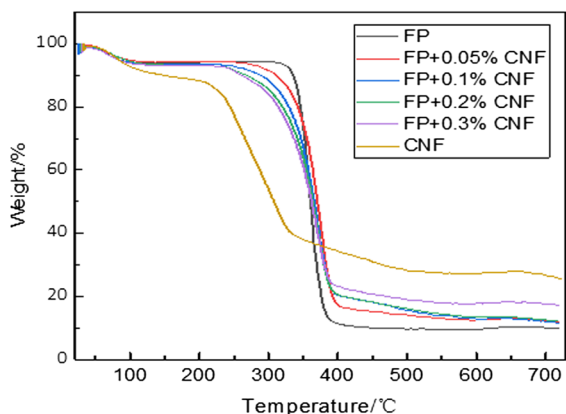
Fig. 8 TG curves of filter paper (FP), CNFs and CNF/FP composite membranes

Table 2 Temperature, acid and alkaline tolerance test of the CNF/FP composite membranes

CNF/FP composite membranes	Pure water flux (L m^{-2} h^{-1})
Untreated	104.20 ± 5.21
High-temperature treatment	1138.66 ± 23.54
Subzero treatment	982.30 ± 20.22
Acid treatment	336.11 ± 9.45
Alkali treatment	210.32 + 10.11

more conducive to intercepting macromolecules. CNCs are short, tend to aggregate and can only be used in the study of microfiltration membranes. The concentration of CNFs is one of the decisive factors that affects the resultant flux of manufactured CNF/FP composite membranes. Higher concentrations resulted in decreased water flux and increased rejection rates. With an increasing amount of added CNFs, the retention rate of bovine serum albumin (BSA) gradually increased to nearly 100% and reached ultrafiltration levels. Different drying methods and different solvent displacement methods also affected the membrane structure, therefore affecting the resultant water flux and retention rate. CNF/FP composite membranes obtained by vacuum drying at 60 °C with 0.1% CNFs showed excellent ultrafiltration properties with retention rates as high as 97.14% and a membrane flux of 46,279 L m^{-2} h^{-1}. The preparation of CNF/FP composite membranes by vacuum drying is direct and simple. Furthermore, the CNF/FP composite filtration material contains electronegative nanocellulose,

which can effectively improve the adsorption and filtration abilities of fine particles. Most importantly, separation membranes with different filtration properties can be designed by controlling the morphology, concentration of nanofibers and the drying process. There is great potential for the application of these composite filtration materials.

References

Baker MN (1981) The quest for pure water: the history of water purification from the earliest records to the twentieth century. American Water Works Association, New York, pp 64–80

Bowen WR, Jenner F (1995) Theoretical descriptions of membrane filtration of colloids and fine particles: an assessment and review. Adv Colloid Interface Sci 56:141–200

Cadotte JE, Petersen RJ, Larson RE et al (1980) A new thin-film composite seawater reverse osmosis membrane. Desalination 32:25–31

Carpenter AW, de Lannoy CF, Wiesner MR (2015) Cellulose nanomaterials in water treatment technologies. Environ Sci Technol 49(9):5277–5287

Chen P, Cho SY, Jin HJ (2010) Modification and applications of bacterial celluloses in polymer science. Macromol Res 18(4):309–320

Chun SJ, Choi ES, Lee EH et al (2012) Eco-friendly cellulose nanofiber paper-derived separator membranes featuring tunable nanoporous network channels for lithium-ion batteries. J Mater Chem 22(32):16618–16626

Ferraz N, Leschinskaya A, Toomadj F et al (2013) Membrane characterization and solute diffusion in porous composite nanocellulose membranes for hemodialysis. Cellulose 20(6):2959–2970

Habibi Y, Chanzy H, Vignon MR (2006) TEMPO-mediated surface oxidation of cellulose whiskers. Cellulose 13(6):679–687

Henmi M, Nakatsuji K, Ichikawa T et al (2012) Self-organized liquid-crystalline nanostructured membranes for water treatment: selective permeation of ions. Adv Mater 24(17):2218

Isogai A, Hänninen T, Fujisawa S et al (2018) Catalytic oxidation of cellulose with nitroxyl radicals under aqueous conditions. Prog Polym Sci 86:122–148

Jakob HF, Fengel D, Tschegg SE et al (1995) The elementary cellulose fibril in *Picea abies*: comparison of transmission electron microscopy, small-angle X-ray scattering, and wide-angle X-ray scattering results. Macromolecules 28(26):8782–8787

Jelen P (1998) Ultrafiltration and microfiltration handbook. Int Dairy J 8(8):76–77

Karan S, Samitsu S, Peng X et al (2012) Ultrafast viscous permeation of organic solvents through diamond-like carbon nanosheets. Science 335(6067):444–447

Karim Z, Mathew AP, Grahn M et al (2014) Nanoporous membranes with cellulose nanocrystals as functional entity in chitosan: removal of dyes from water. Carbohydr Polym 112:668–676

Karim Z, Claudpierre S, Grahn M et al (2016) Nanocellulose based functional membranes for water cleaning: tailoring of mechanical properties, porosity and metal ion capture. J Membr Sci 514:418–428

Klemm D, Heublein B, Fink HP et al (2005) Cellulose: fascinating biopolymer and sustainable raw material. Angew Chem Int Ed 44(22):3358–3393

Klemm D, Kramer F, Moritz S et al (2011) Nanocelluloses: a new family of nature-based materials. Angew Chem Int Ed 50(24):5438–5466

Kong L, Zhang D, Shao Z et al (2014) Superior effect of TEMPO-oxidized cellulose nanofibrils (TOCNs) on the performance of cellulose triacetate (CTA) ultrafiltration membrane. Desalination 332(1):117–125

Ling S, Chen W, Fan Y et al (2018a) Biopolymer nanofibrils: structure, modeling, preparation, and applications. Prog Polym Sci 85:1–56

Ling S, Kaplan DL, Buehler MJ (2018b) Nanofibrils in nature and materials engineering. Nat Rev Mater 3:18016

Liu T, Zhou H, Graham N et al (2018) The antifouling performance of an ultrafiltration membrane with pre-deposited carbon nanofiber layers for water treatment. J Membr Sci 557:87–95

Lv J, Zhang G, Zhang H et al (2018) Improvement of antifouling performances for modified PVDF ultrafiltration membrane with hydrophilic cellulose nanocrystal. Appl Surf Sci 440:1091–1100

Ma H, Yoon K, Rong L et al (2010) High-flux thin-film nanofibrous composite ultrafiltration membranes containing cellulose barrier layer. J Mater Chem 20(22):4692–4704

Ma H, Burger C, Hsiao BS et al (2011a) Ultra-fine cellulose nanofibers: new nano-scale materials for water purification. J Mater Chem 21(21):7507–7510

Ma H, Burger C, Hsiao BS et al (2011b) Nanofibrous microfiltration membrane based on cellulose nanowhiskers. Biomacromolecules 13(1):180–186

Ma H, Burger C, Hsiao BS et al (2014) Fabrication and characterization of cellulose nanofiber based thin-film nanofibrous composite membranes. J Membr Sci 454(6):272–282

Mautner A, Lee KY, Lahtinen P et al (2014) Nanopapers for organic solvent nanofiltration. Chem Commun 50(43):5778–5781

Mautner A, Lee KY, Tammelin T et al (2015) Cellulose nanopapers as tight aqueous ultra-filtration membranes. React Funct Polym 86:209–214

Moon RJ, Martini A, Nairn J et al (2011) Cellulose nanomaterials review: structure, properties and nanocomposites. Chem Soc Rev 40(7):3941–3994

Mungray AA, Murthy ZVP (2012) Comparative performance study of four nanofiltration membranes in the separation of mercury and chromium. Ionics 18(8):811–816

Nishino T, Takano K, Nakamae K (1995) Elastic modulus of the crystalline regions of cellulose polymorphs. J Polym Sci Part B Polym Phys 33(11):1647–1651

Pesek SC, Koros WJ (1994) Aqueous quenched asymmetric polysulfone hollow fibers prepared by dry/wet phase separation. J Membr Sci 88(1):1–19

Saito T, Nishiyama Y, Putaux JL et al (2006) Homogeneous suspensions of individualized microfibrils from TEMPO-catalyzed oxidation of native cellulose. Biomacromolecules 7(6):1687–1691

Siró I, Plackett D (2010) Microfibrillated cellulose and new nanocomposite materials: a review. Cellulose 17(3):459–494

Soeta H, Fujisawa S, Saito T et al (2015) Low-birefringent and highly tough nanocellulose-reinforced cellulose triacetate. ACS Appl Mater Interfaces 7(20):11041–11046

Sun B, Hou Q, Liu Z et al (2015) Sodium periodate oxidation of cellulose nanocrystal and its application as a paper wet strength additive. Cellulose 22(2):1135–1146

Thakur VK, Voicu SI (2016) Recent advances in cellulose and chitosan based membranes for water purification: a concise review. Carbohydr Polym 146:148–165

Van Reis R, Zydney A (2001) Membrane separations in biotechnology. Curr Opin Biotechnol 12(2):208–211

Wang R, Guan S, Sato A et al (2013) Nanofibrous microfiltration membranes capable of removing bacteria, viruses and heavy metal ions. J Membr Sci 446:376–382

Wang Z, Crandall C, Prautzsch VL et al (2017) Electrospun regenerated cellulose nanofiber membranes surface-grafted with water-insoluble poly (HEMA) or water-soluble poly (AAS) chains via the ATRP method for ultrafiltration of wate. ACS Appl Mater Interfaces 9(4):4272–4278

Wessling M, Lopez ML, Strathmann H (2001) Accelerated plasticization of thin-film composite membranes used in gas separation. Sep Purif Technol 24(1–2):223–233

Xu X, Yang YQ, Xing YY et al (2013) Properties of novel polyvinyl alcohol/cellulose nanocrystals/silver nanoparticles blend membranes. Carbohydr Polym 98(2):1573–1577

Yang N, Zhang W, Ye C et al (2018) Nanobiopolymers fabrication and their life cycle assessments. Biotechnol J 1700754:1–13

Yano H, Sugiyama J, Nakagaito A et al (2010) Optically transparent composites reinforced with networks of bacterial nanofibers. Adv Mater 17(2):153–155